Research Square

Preprints are preliminary reports that have not undergone peer review.
They should not be considered conclusive, used to inform clinical practice,
or referenced by the media as validated information.

Mesoscopic mapping of the visual pathway in a female 5XFAD mouse model of Alzheimer's disease

Yunkwon Nam
Konyang University College of Medicine
Sujin Kim
Konyang University College of Medicine
Jieun Kim
Korea Brain Research Institute
Hyang-Sook Hoe
Korea Brain Research Institute
Minho Moon (hominmoon@konyang.ac.kr)
Konyang University College of Medicine https://orcid.org/0000-0002-8140-5928

Research Article

Keywords: Alzheimer's disease, visual pathway, 5XFAD mice, cholera toxin β subunits

Posted Date: April 26th, 2022

DOI: https://doi.org/10.21203/rs.3.rs-1548492/v1

License: This work is licensed under a Creative Commons Attribution 4.0 International License.
Read Full License

Abstract

Synaptic and network disruption is correlated with cognitive decline and loss of sensation in Alzheimer's disease (AD). Surprisingly, amyloid-β (Aβ) deposition and Aβ-induced neurodegeneration appear in the retina at the early-stage of AD. Although these Aβ-related changes in the retina could cause damage to the visual functions, no studies have yet revealed the alteration in the visual pathway of AD. Therefore, we investigated the alteration of visual circuits in the AD mouse model using anterograde neurotracer. We investigated the Aβ accumulation by immunofluorescent staining in the retina and retinorecipient areas of 4- and 12-month-old female 5XFAD transgenic mice. Following intravitreal injection of cholera toxin β subunits (CTβ) tracer, we evaluated the fluorescence intensity of accumulated CTβ in the retinorecipient areas in 4- and 12-month-old female wild-type and 5XFAD mice. Our results demonstrated that Aβ accumulation occurred in the retina and retinorecipient regions of early and late stages of the 5XFAD mice. Retinal efferents to the suprachiasmatic nucleus and lateral geniculate nucleus were impaired in the early-stage of AD. Moreover, retinal connections to the dorsal lateral geniculate nucleus and superior colliculus were degenerated in the late-stage of AD. Although these results provide the first neuroanatomical evidence for decreased visual connectivity in an AD mouse model, it is difficult to explain cell type-specific connectivity. These findings reveal the Aβ-induced visual circuit disturbances at the mesoscale level in both the early and late stages of AD and provide anatomical and functional insights into the visual circuitry of AD.

Introduction

Alzheimer's disease (AD) is characterized by increased accumulation of amyloid plaques, composed primarily of 36–43 residue amyloid-β (Aβ) peptides, in the brains of the patients with AD [1, 2]. Notably, the intermediate and soluble oligomer Aβ forms provoke neuronal death and synaptic loss in the brain [3]. Moreover, the neurotoxic and synaptotoxic Aβ directly attenuates the neural circuit networks in the brains affected by AD [4–7]. These impairments in various neural circuits and brain networks that underlie cognitive, behavioral, and sensory systems could result in cognitive decline, emotional deficit, and sensory loss in AD [8]. Unfortunately, current Aβ-centered pharmacologic therapies have demonstrated limited efficacy in the treatment of AD [9]. These limitations imply that establishing a neural circuit-centered therapeutic approach directly related to AD-associated cognitive decline and sensory impairment could be effective for the treatment of AD. Therefore, it is important to understand which neural circuits are altered and damaged in the brains with AD.

Visual function impairment is common in patients with AD [10]. It has been known that AD-related pathology affects vision-related structures and visual system impairment is associated with the pathogenesis of AD.[11–14] Accumulations of Aβ and hyperphosphorylated tau in the retina precede the deposits of Aβ plaques in the brains of AD mouse models [13, 14]. Moreover, damage to the inner retina by Aβ aggregation precedes neuronal cell death and cognitive impairment in AD [14]. Similarly, Aβ accumulation and neuronal degeneration in the retina were significantly increased in patients with AD compared with age-matched controls [15]. Notably, retinal nerve fiber layer (RNFL) and retinal ganglion

cell (RGC) degeneration was observed in the retina of patients with AD, and the intrinsically photosensitive retinal ganglion cells (ipRGCs), a subset of RGCs, were severely damaged [16–18]. Thus, the detriment of the inner retina by Aβ is closely related to RGC degeneration and the overall reduction in the axon of RGCs. Moreover, the inner retina and RNFL undergo extensive damage in the early stage of AD without visual failure [19, 17]. Surprisingly, it has been reported that a thinner RNFL is linked to cognitive impairment in patients with mild cognitive impairment (MCI) and AD [16]. Considered together, Aβ-induced deficiency of RGCs and RNFLs is prominent in the early stage of AD, and these deficiencies result in the deterioration of the visual pathways from the eye to the brain.

In the brain, retinorecipient areas originating from the eye include 25 ipsilateral brain regions and 34 contralateral brain regions [20]. The representative retinorecipient areas are the lateral geniculate nucleus (LGN), superior colliculus (SC), suprachiasmatic nucleus (SCN), olivary pretectal nucleus (OPN), and medial terminal nucleus of the accessory optic tract (MTN) [21]. The LGN is divided into subregions, such as the dorsal lateral geniculate nucleus (dLGN), intergeniculate leaflet (IGL), and ventral lateral geniculate nucleus (vLGN) [22]. In particular, the dLGN is related to vision and the IGL and vLGN are related to visuomotor, vestibular, ocular, and circadian functions [22]. Ninety percent of the projections from the RGC reach the SC, and these connections are involved in eye movement and vision [23–25]. SCN and OPN receive inputs from the ipRGCs and control the circadian rhythm and pupillary light reflexes, respectively [26]. The MTN is connected with the ON direction-selective ganglion cells (DSGCs) specialized in stabilizing images [20]. Surprisingly, in the early stage of AD progression, pathophysiologic alteration occurs in vision-related brain areas, which causes visual pathway and function impairment in AD. The AD-related visual deficits include loss of visual field, decreased contrast sensitivity, low visual acuity, impaired color vision or motion perception, visuospatial difficulties, object agnosia, prosopagnosia, and impaired identification of emotional facial expressions [10]. Thus, impairment in the connectivity of the retina with retinorecipient areas may affect the provocation of visual dysfunction in AD.

Although the connectivity between retina and retinorecipient regions in the healthy brain is well known, no studies the alterations of the visual pathways in the brains with AD. Moreover, it has been shown that Aβ-induced deficiency of RGC and RNFL appears in the early stages of AD, resulting in visual pathway impairment. Therefore, a hypothesis was formulated stating that the visual pathway could be altered in Aβ-overexpressing transgenic mice before cognitive decline. To reveal the connection of the retina with retinorecipient areas, we used non-transsynaptic anterograde neural tracer and performed histological analysis in both 4-month-old 5XFAD mice corresponding to the prodromal AD [27] and 12-month-old 5XFAD mice corresponding to the severe AD [28].

Materials And Methods

Animals

The 5XFAD (five familial AD mutations) mice express three mutations in the human *APP* gene (FloridaV717I, SwedishK670N/M671L, and LondonI716V) and two mutations in the human *PSEN1* gene (L286V and M146L). The animals were purchased from the Jackson Laboratory in Bar Harbor, Mainer, ME, USA (#006554). The present study used 4- and 12-month-old female 5XFAD mice and wild-type (WT) littermates. As previously described [29], the 5XFAD transgenic mice were identified through genotyping of tail DNA. Moreover, some 5XFAD and WT littermate mice start to exhibit retinal degeneration and lose sight at 35 days of age as a result of phosphodiesterase-6b retinal degeneration-1 (*Pde6b*^{rd1}) allele in the SJL/J background strain [30]. *Pde6b*^{rd1} has an autosomal recessive inheritance pattern [31]. Thus, mice with retinal degeneration *Pde6b*^{rd1} mutation were classified and excluded using genotyping (Mutant: 5-AAG CTA GCT GCA GTA ACG CCA TTT-3, Wild-type: 5-ACC TGC ATG TGA ACC CAG TAT TCT ATC-3, Common: 5-CTA CAG CCC CTC TCC AAG GTT TAT AG-3). WT and 5XFAD mice excluding *Pde6b*^{rd1} mutants were randomly assigned into four groups: (1) 4-month-old WT mice (n = 5), (2) 4-month-old 5XFAD mice (n = 5), (3) 12-month-old WT mice (n = 5), and (4) 12-month-old 5XFAD mice (n = 5). Maintenance and treatment of the animals were performed as per the principles of the Care and Use of Laboratory Animals (NIH Publication No. 85 – 23, revised 1985) and the Animal Care and Use Guidelines of Konyang University (Project code: P-18-06-A-01). Every attempt was made to keep the number of animals utilized and their suffering to a minimum.

Intravitreal Injections

All the animals were anesthetized with a dose of 250 μg/kg Avertin (Tribromoethanol; Sigma-Aldrich, St. Louis, MO, USA). The intravitreal injection was performed using a microscope (Leica, stereozoom S9 D). A sharp 30-gauge needle was inserted into the edge of the right eye to make a small incision and 1 μL of vitreous fluid was subsequently withdrawn using a blunt 33-gauge needle attached to a Hamilton syringe. Finally, 1 μL of 1 mg/mL cholera toxin β subunit (CTβ) conjugated to Alexa-Fluor 488 (Thermo Fisher Scientific Inc., Waltham, MA, USA) was injected into the right eye using the same Hamilton syringe [13]. In order to prevent eye damage, a needle was placed between the lens and the retina, eye ointment was applied following the intravitreal injection.

Brain Tissue and Retina Wholemount Preparation

The animals were anesthetized three days following the CTβ injections, transcardially perfused with 0.05 M phosphate-buffered saline (PBS), and subsequently fixed with cold 4% paraformaldehyde in 0.1 M phosphate buffer (PB). Thereafter, the eyes and brain tissues were extracted, and the tissues were post-fixed in 0.1 M PB containing 4% paraformaldehyde for 20 h at 4°C. For cryoprotection, the brains were subsequently immersed in 30% sucrose in 0.05 M PBS solution for 3 days at 4°C. The brains were subsequently embedded in Surgipath® frozen section compound (Leica Biosystems, Wetzlar, Germany) and sliced into serial 30-μm-thick coronal slices using a CM1850 cryostat (Leica Biosystems). As previously described [32], for the retina wholemount preparation, the eye tissues were dissected to remove the lens and vitreous, and the retina was collected. Then, quadrants of the retina were cut and spread flat on the glass.

Immunofluorescence Labeling

To investigate the immunoreactivity of Aβ accumulation, the retina and brain tissues were incubated using a blocking solution (0.05% bovine serum albumin, 1.5% normal goat serum, and 0.3% Triton X-100 in PBS) and mouse anti-4G8 antibody (1:2,000; BioLegend, San Diego, CA, USA) overnight at 4°C. And then, the retina and brain tissues were incubated with donkey Alexa 594-conjugated anti-mouse IgG (1:200; Thermo Fisher Scientific Inc., Waltham, MA, USA) for 1 h at room temperature. To counterstain the nuclei, the retina and brain tissues were mounted on ProbeOnTM Plus Microscope Slides (Thermo Fisher Scientific Inc.) and covered with Fluoroshield™ with 4',6-diamidino-2-phenylindole (DAPI) (Sigma-Aldrich).

Image Acquisition and Analysis

All the brain and retinal tissues labeled with CTβ and 4G8 staining were imaged using a Zeiss LSM 700 Meta confocal microscope (Carl Zeiss AG, Oberkochen, Germany). The images of the CTβ-labeled cell bodies and axon terminals and 4G8-positve Aβ were quantified in the retina and retinorecipient regions using ImageJ software (NIH, Bethesda, MD, USA). The images of the CTβ-labeled axon terminals were expressed as the fluorescence intensity in arbitrary unit. Values from the four groups were normalized to the controls using the following equations: % of control = (fluorescence intensity of WT or 5XFAD mice/fluorescence intensity average of WT mice) × 100. The immunoreactivity of 4G8 staining was quantified as area fractions of immune-reactive signals in the retina.

Statistical Analysis

All the data were analyzed by GraphPad Prism 7 (Systat Software, La Jolla, CA, USA). Analyzed values are plotted as mean ± standard error of the mean (SEM). Data were analyzed using independent t-tests between the two groups and one-way analysis of variance was performed between the four groups followed by Tukey's post-hoc tests. A *p*-value of less than 0.05 was considered statistically significant. Image acquisition, quantification, and statistical analysis of each group were blindly performed.

Results

Histological profiling of the Aβ accumulation and retinal projections to the brain

To investigate the retinorecipient areas and retinal pathways in the brain with AD, we injected CTβ, a non-transsynaptic anterograde trace, into the vitreous of WT and 5XFAD mice (Fig. 1a). Three days following the intravitreal injection, fluorescence of CTβ conjugated to Alexa-Fluor 488 was detected in the retina of WT and 5XFAD mice (Fig. 1b). Next, we investigated the subcellular localization of CTβ in the retinal flat mount using Z-stack imaging. CTβ fluorescence signals were localized in the cytoplasm of retinal cells stained with DAPI (Fig. 1c-e). Moreover, to examine whether Aβ accumulations were deposited in the retinal RGCs, we injected CTβ and then immunofluorescence staining was conducted using anti-4G8 antibody of 4 month- and 12-month-old 5XFAD mice. We found that Aβ peptides were more aggregated in

the retina of 12-month-old of 5XFAD compared with 4-month-old 5XFAD mice (Fig. 1f). These data suggest that Aβ expression is responsible for retinal RGC-associated Aβ pathology in 4-month-old 5XFAD and that the burden of Aβ plaques is more severe in 12-month-old 5xFAD mice. Subsequently, we examined the retinal efferents to the brain regions of the healthy and AD animals. Consistent with previous studies to elucidate the retinorecipient areas [20, 21]. the signals of CTβ axonally transported from retina were detected in retinorecipient areas, including SCN, OPN, LGN, SC, and MTN of WT and 5XFAD mice (Fig. 2d, f, g). Particularly, the fluorescent CTβ was localized in the terminal button of the axon of the WT and 5XFAD mice (Fig. 2c), which suggests that the CTβ-positive axon terminals originated in the retina. Moreover, we characterized Aβ deposition in retinorecipient areas of 4- and 12-month-old 5XFAD mice (Fig. 2e, h-k). Aβ accumulation was not observed in the SCN, SC, and MTN of 4- and 12-month-old 5XFAD mice (Fig. 2e, i, k). Interestingly, Aβ accumulation was not detected in the OPN of 4-month-old 5XFAD mice, whereas Aβ deposition was observed in 12-month-old 5XFAD mice (Fig. 2h). The LGN showed Aβ deposition in both 4- and 12-month-old 5XFAD mice, demonstrating an age-dependent increase (Fig. 2j). Consequently, we found CTβ-labeled axon terminals in retinorecipient regions in the brains of WT and 5XFAD mice, and that the patterns and degrees of Aβ accumulation vary across regions and phases of AD progression in retinorecipient areas.

Disruption of the retina-SCN connections in animal model of AD

It is well-known that the RGCs project to the SCN of the hypothalamus [33]. In particular, ipRGCs primarily send information to the SCN [26, 34, 35]. In order to visualize the neural connections from the retina to the SCN, we injected CTβ into the vitreous of 4- and 12-month-old WT and 5XFAD mice. CTβ-positive signals were detected in the SCN of all the mouse groups (Fig. 3a, b). To examine whether the retina-SCN pathway is altered in Aβ-overexpressing brains, we compared the fluorescence signals of CTβ in the SCN of the 5XFAD and WT mice (Fig. 3c). The fluorescence intensity of CTβ in the SCN was significantly reduced in 4-month-old 5XFAD mice compared with WT mice of the same age (Fig. 3c, d). However, in 12-month-old 5XFAD mice, there was no significant difference in the CTβ fluorescence intensity compared to WT mice of the same age (Fig. 3c, d). Moreover, anterograde tracing results showed that in the SCN, CTβ fluorescence intensity of 12-month-old WT mice was significantly lower than that of 4-month-old WT mice (Fig. 3d). These results suggest that efferent projections from the retina to the SCN are impaired before the onset of cognitive decline and by normal aging.

Tracing the retina-OPN pathways in the 5XFAD mice

To investigate whether the retinal outputs to OPN are altered in Aβ-overexpressing brains, we traced the transport of the anterograde tracer from the retina to the OPN in the 4- and 12-month-old WT and 5XFAD mice (Fig. 4a, b). There was no difference in the fluorescence intensity of CTβ between WT and 5XFAD mice at the age of 4 months (Fig. 4c). Similarly, there was no difference of fluorescence intensity of CTβ between 12-month-old WT and 5XFAD mice (Fig. 4c). Moreover, the retina-OPN connectivity did not show

age-related impairment in WT mice (Fig. 4d). Consequently, our findings demonstrate that the retina-OPN pathway is rarely altered by AD progression and normal aging.

Decreased retina-LGN connectivity in the 5XFAD mice

The LGN is a crucial region in the visual pathway that relays visual information from the retina to the primary visual cortex [36]. We analyzed CTβ-positive signals in the three subregions of LGN, such as dLGN, IGL, and vLGN, in 4- and 12-month-old WT and 5XFAD groups (Fig. 5a, b). First, compared to the 4- and 12-month-old WT mice, the CTβ-labeled efferent from the retina to dLGN were significantly decreased in the 4- and 12-months-old 5XFAD mice, individually (Fig. 5c), which indicated that the retinal projections to dLGN were damaged by AD progression. The comparison of the CTβ-positive areas in the dLGN between 4- and 12-month-old WT mice did not show any degeneration with aging (Fig. 5f). Second, CTβ-labeled axons in the IGL were significant decreased in the 4-month-old 5XFAD mice compared to the 4-month-old WT mice (Fig. 5d); however, there was no difference in the fluorescence intensity between the WT and 5XFAD mice at the age of 12 months (Fig. 5d). Normal aging significantly damaged the retina-IGL pathway, whereas AD progression did not alter the retina-IGL projections (Fig. 5f). Finally, the anterograde-tracing from the retina to the vLGN demonstrated that the CTβ-positive axon terminals were significantly decreased in the 4-month-old 5XFAD compared to 4-month-old WT mice (Fig. 5e); however, there were no differences in the alteration of the retina-vLGN connectivity between 12-month-old WT and 5XFAD mice (Fig. 5e). Surprisingly, both normal aging and AD progression significantly disrupted the retina-vLGN pathway (Fig. 5f). Taken together, these findings demonstrate (1) that the retinal efferents to dLGN, IGL, and vLGN are severely damaged in the AD brain even before the onset of cognitive decline, and (2) the significant alteration of the eye-LGN connection during AD progression as well as normal aging.

Altered retina-SC connection in the Aβ-overexpressing mice

The SC is a region that relays visual information as part of the extrageniculate visual pathway from the retina to the higher visual cortex and plays an important role in visual function [37]. To reveal the retina-SC pathway, we conducted anterograde-tracing with CTβ in 4- and 12-month-old WT and 5XFAD mice (Fig. 6a, b). There was no impairment in the retina-SC pathway of 4-month-old 5XFAD mice compared to the 4-month-old WT mice (Fig. 6c). In contrast, the retina-SC connection of 12-month-old 5XFAD mice was significantly reduced compared to that of the 12-month-old WT mice (Fig. 6c). Moreover, comparison of CTβ-positive axon terminals between 4-month-old and 12-month-old mice showed a significant age-related decrease in the retina-SC projection of both WT and 5XFAD mice (Fig. 6d). Therefore, these anterograde-tracing results demonstrate that the retina-SC projection is impaired during normal aging and AD progression.

Decreased retina-MTN projections in the animal model of AD

To reveal the changes in connectivity from the retina to the MTN in an AD mouse model, we detected the CTβ-positive signals in MTN of 4- and 12-month-old WT and 5XFAD groups (Fig. 7a, b). Compared to both the 4- and 12- month-old WT mice, the CTβ-labeled efferents from the retina were not reduced in the MTN of 4- and 12- month-old 5XFAD mice (Fig. 7c). Conversely, the retina-MTN pathway was significantly decreased in the 12- month-old WT and 5XFAD mice, compared to the 4-month-old WT and FAD mice, respectively (Fig. 7d). Taken together, these results suggest that retina-SC pathways significantly degenerate during aging and AD progression.

Discussion

Although visual circuit impairments in patients with AD patients has been reported at the macroscopic level [38], to the best of our knowledge, there is no study on the alteration of the visual circuit at the mesoscale level in the AD brain. Thus, our study aimed to provide direct anatomical evidence in a mouse model of AD by examining the topographical changes in various visual pathways of AD progression. To investigate the visual circuitry of the AD brain, we intravitreally injected a non-transsynaptic anterograde trace CTβ into the eyes of 4- and 12-month-old WT and 5XFAD mice. We demonstrated that the retinal projections to the SCN, dLGN, IGL, and vLGN reduced in the 4-month-old 5XFAD mice, which exhibit no cognitive decline, compared with the 4-month-old WT mice. In addition, we found decreased connections of retina-dLGN and retina-SC in the 12-month-old 5XFAD mice, representing severe stage of AD, compared to 12-month-old WT mice. Finally, we revealed that retinal connectivity decreases in several retinorecipient areas except for the OPN by normal aging. The present study demonstrated for the first time, the alteration of the visual pathways from the retina in the AD brain at the mesoscale level (Fig. 8).

It is well known that Aβ-induced neuronal dysfunctions induces neuronal circuit and network disturbances [39]. A key component of these neuronal dysfunctions is axonal degeneration. Axonal degeneration by Aβ toxicity preceded neuronal cell death. In addition, inhibition of axonal degeneration through overexpression of nicotinamide mononucleotide adenylyltransferase 1 (Nmnat1) and Bcl-xl prevented neuronal cell death [40]. This evidence suggests that Aβ targets the axon rather than the soma. Therefore, Aβ observed in the retina (Fig. 1f) can cause axonal degeneration of RGCs, resulting in disruption of the visual pathway. Damage to neuronal circuits leads to functional dysfunctions. Many visual-related dysfunctions have been reported in patients with AD and animal models [41, 42]. More than half of the patients with AD suffer from sleep disorders [41]. Moreover, circadian rhythm disturbance was observed in 4-month-old 5XFAD mice [42]. The accompanying circadian disruption in patients with AD and an animal model is closely related to the SCN, vLGN, and IGL [43, 44]. Surprisingly, the connections between the retina and the SCN, vLGN, and IGL were significantly impaired in the 4-month-old 5XFAD mice (Fig. 3c and 5d, e). These results suggest that the visual pathways in the SCN, vLGN, and IGL are severely impaired in the early-stage of AD, and the alteration of these circuitry results in abnormal circadian rhythms. In addition, it is well known that the dLGN is involved in the control of color vision and contrast sensitivity [45, 46]. Loss of contrast sensitivity and impairment of color vision is one of the early symptoms in patients with AD [47, 48]. Moreover, a study using an APPSWE/PS1ΔE9 mouse model reported that contrast sensitivity and color vision were impaired in AD progression [49]. Similarly,

projection from the retina to the dLGN decreased in the 4- and 12-month-old 5XFAD mice (Fig. 5c, f). This finding indicated that the retina-dLGN pathway impaired AD progress, and the impairment of these circuitry resulted in the loss of contrast sensitivity and color vision. The SC is involved in visuomotor function, such as eye movement [23, 25]. Interestingly, visuomotor impairment was observed from 6 months of age in 5XFAD mice [50]. Our results did not show the altered pathway from the retina to the SC in 4-month-old 5XFAD mice. In contrast, the retina-SC pathway was significantly reduced in 12-month-old 5XFAD mice (Fig. 6c, d). This finding demonstrates that retina-to-SC projections initiate impairment at the late stage of AD, and the disruption of retina-SC circuitry causes visuomotor dysfunction.

In the early-stage of Aβ-overexpressing mice, the circuits from the retina to SCN and LGN are impaired (Figs. 3 and 5), and the RGCs constituting these circuits are mainly ipRGCs [21]. Specifically, M1 ipRGCs expressing the Brn3b transcription factor innervate into the dLGN and vLGN, and Brn3b-negative M1 ipRGCs project into the SCN and IGL [26]. In addition, cadherin-6-expressing ipRGCs output to IGL and vLGN [51]. Thus, these evidences suggest that Aβ-induced impairments of Brn3b-negative and positive M1 ipRGCs and their axons could be predominant in the early-stage of AD. In the late-stage of Aβ-overexpressing mice, pathways from the retina to the dLGN and SC are impaired (Fig. 5c and 6), these pathways consist of various RGCs axons [21]. The dLGN receives inputs from a variety of RGCs, such as on, off, and on-off DSGCs and off alpha RGCs [22]. Eighty to ninety percent of RGCs reach the SC [24]. Based on several studies, most RGCs and their innervation could be impaired by various AD pathologies in the late-stage of AD.

Neurodegenerative biomarkers for detecting cognitive decline or MCI developing dementia is critical [52]. One of the studies reports that ophthalmological examinations have revealed many visual alterations in individuals with neurodegenerative disease [53]. Visual indications commonly precede brain symptoms in some disorders, suggesting that eye examinations could provide earlier detection of the underlying disease [11]. Our results demonstrated that Aβ accumulation in the retina and impairment of visual pathways appear before the cognitive decline (Fig. 1f, 3d, and 5f). These results suggest that impaired retinas could be utilized to promptly diagnose AD in the early stage of the disease progression. Surprisingly, advances in ophthalmologic techniques for the study of the retina *in vivo* enable the diagnosis of AD through retinal degeneration. A non-invasive and inexpensive method of diagnosing AD through the retina can make a huge contribution to AD treatment. A recent review article presents several ocular biomarkers studied in patients with AD, such as decreased RNFL thickness, retinal vascular changes, and AD pathology detection in the retina [54]. In addition to the diagnosis through retinal degeneration, various biomarkers exist that diagnose AD by measuring the visual dysfunction [55–58].

Our results suggested the retinal outputs were impaired in the 5XFAD mice. In particular, the most common neurotransmitter in the visual system, including the retina, is glutamate [59]. Unfortunately, most conventional tracers are unable to reveal the connectivity at the level of the cell-type-specific pathway [60]. Therefore, genetic tracing using cell-type-specific promoters should be used to investigate the disruption of glutamate-specific visual pathways. Nevertheless, the current research is the first to demonstrate the alteration in the visual pathways in an animal model of AD at the mesoscale level.

Restoring damaged visual pathways with optogenetic stimulation, based on mesoscopic mapping of connectivity in the AD brain, could be a possible therapeutic approach for treating visual symptoms in patients with AD.

5XFAD mouse, an Aβ-overexpressing mouse model, has a high level of $A\beta_{40}$ and $A\beta_{42}$ peptide, which is the closest to humans in the retina and brain. Moreover, the 5XFAD mice showed stronger retinal and synaptic pathology than other AD mouse models [61]. Significantly increased Aβ concentrations were observed in the eyes of young 5XFAD mice without cognitive impairment compared to WT mice of the same age [14, 62, 63]. In addition, visual behavior abnormalities and circadian rhythm disturbance were reported in 5XFAD mice [42, 50]. Unfortunately, 5XFAD mice do not reflect all of the pathologies of AD and may not reflect the same visual pathway impairment as patients with AD. Nevertheless, since non-clinical studies are needed for developing treatment and diagnostic methods for AD, among various AD models, we chose 5XFAD mice, which accumulate the Aβ in the retina at the early-stage and exhibit visual-related symptoms.

Conclusion

In this study, we examined the alteration of the visual pathway in the animal model of AD at the mesoscale level in both the early and late stages of AD. Taken together, the results of our study using 5XFAD mice demonstrated that (1) retinal projections to the SCN, dLGN, IGL, and vLGN were significantly impaired in the early stages of AD, (2) connections of the retina with dLGN and SC were disrupted in the late stages of AD, (3) the visual pathways in the brain with AD showed a trend towards accelerated degeneration during the AD progression, and (4) the visual circuits in the healthy brain degenerated according to aging.

Declarations

Acknowledgments: The authors thank all participants involved in this study.

Contributors: Y. N., S.K., J. K., H-S. H., and M. M. designed the study. Y. N., S.K., and J. K. acquired and analyzed the data. Y. N., S.K., J. K., H-S. H., and M. M. wrote the article. All authors have read and agreed to the published version of the manuscript.

Funding: This research was funded by Basic Science Research Program of the National Research Foundation of Korea (NRF), which is funded by the Ministry of Science, ICT & Future Planning (NRF-2018R1D1A3B07041059) and was supported by a grant of the Korea Health Technology R&D Project through the Korea Health Industry Development Institute (KHIDI), funded by the Ministry of Health & Welfare, Republic of Korea (grant number: HF21C0021). This work was also supported by the KBRI basic research program through KBRI funded by the Ministry of Science, ICT & Future Planning (grant number 22-BR-02-03).

Data Availability: All data discovered and analyzed during this study are included in this manuscript.

Ethics approval: Not applicable.

Consent to participate: Not applicable.

Consent for publication: Not applicable.

Competing interests: None declared.

References

1. Querfurth HW, LaFerla FM (2010) Alzheimer's disease. N Engl J Med 362 (4):329-344. doi:10.1056/NEJMra0909142
2. O'Brien RJ, Wong PC (2011) Amyloid precursor protein processing and Alzheimer's disease. Annu Rev Neurosci 34:185-204. doi:10.1146/annurev-neuro-061010-113613
3. Walsh DM, Selkoe DJ (2007) A beta oligomers - a decade of discovery. J Neurochem 101 (5):1172-1184. doi:10.1111/j.1471-4159.2006.04426.x
4. Kim S, Nam Y, Jeong YO, Park HH, Lee SK, Shin SJ, Jung H, Kim BH, Hong SB, Park YH, Kim J, Yu J, Yoo DH, Park SH, Jeon SG, Moon M (2019) Topographical Visualization of the Reciprocal Projection between the Medial Septum and the Hippocampus in the 5XFAD Mouse Model of Alzheimer's Disease. Int J Mol Sci 20 (16). doi:10.3390/ijms20163992
5. Canter RG, Penney J, Tsai LH (2016) The road to restoring neural circuits for the treatment of Alzheimer's disease. Nature 539 (7628):187-196. doi:10.1038/nature20412
6. Jeon SG, Kim YJ, Kim KA, Mook-Jung I, Moon M (2018) Visualization of Altered Hippocampal Connectivity in an Animal Model of Alzheimer's Disease. Mol Neurobiol 55 (10):7886-7899. doi:10.1007/s12035-018-0918-y
7. Kim S, Nam Y, Kim Hs, Jung H, Jeon SG, Hong SB, Moon M (2022) Alteration of Neural Pathways and Its Implications in Alzheimer’s Disease. Biomedicines 10 (4):845
8. Albers MW, Gilmore GC, Kaye J, Murphy C, Wingfield A, Bennett DA, Boxer AL, Buchman AS, Cruickshanks KJ, Devanand DP, Duffy CJ, Gall CM, Gates GA, Granholm AC, Hensch T, Holtzer R, Hyman BT, Lin FR, McKee AC, Morris JC, Petersen RC, Silbert LC, Struble RG, Trojanowski JQ, Verghese J, Wilson DA, Xu S, Zhang LI (2015) At the interface of sensory and motor dysfunctions and Alzheimer's disease. Alzheimers Dement 11 (1):70-98. doi:10.1016/j.jalz.2014.04.514
9. Jeremic D, Jiménez-Díaz L, Navarro-López JD (2021) Past, present and future of therapeutic strategies against amyloid-β peptides in Alzheimer’s disease: a systematic review. Ageing Research Reviews 72:101496. doi:https://doi.org/10.1016/j.arr.2021.101496

10. Lenoir H, Sieroff E (2019) [Visual perceptual disorders in Alzheimer's disease]. Geriatr Psychol Neuropsychiatr Vieil 17 (3):307-316. doi:10.1684/pnv.2019.0815
11. London A, Benhar I, Schwartz M (2013) The retina as a window to the brain-from eye research to CNS disorders. Nat Rev Neurol 9 (1):44-53. doi:10.1038/nrneurol.2012.227
12. Kusne Y, Wolf AB, Townley K, Conway M, Peyman GA (2017) Visual system manifestations of Alzheimer's disease. Acta Ophthalmol 95 (8):e668-e676. doi:10.1111/aos.13319
13. Chiasseu M, Alarcon-Martinez L, Belforte N, Quintero H, Dotigny F, Destroismaisons L, Vande Velde C, Panayi F, Louis C, Di Polo A (2017) Tau accumulation in the retina promotes early neuronal dysfunction and precedes brain pathology in a mouse model of Alzheimer's disease. Mol Neurodegener 12 (1):58. doi:10.1186/s13024-017-0199-3
14. Criscuolo C, Cerri E, Fabiani C, Capsoni S, Cattaneo A, Domenici L (2018) The retina as a window to early dysfunctions of Alzheimer's disease following studies with a 5xFAD mouse model. Neurobiol Aging 67:181-188. doi:10.1016/j.neurobiolaging.2018.03.017
15. Koronyo Y, Biggs D, Barron E, Boyer DS, Pearlman JA, Au WJ, Kile SJ, Blanco A, Fuchs DT, Ashfaq A, Frautschy S, Cole GM, Miller CA, Hinton DR, Verdooner SR, Black KL, Koronyo-Hamaoui M (2017) Retinal amyloid pathology and proof-of-concept imaging trial in Alzheimer's disease. JCI Insight 2 (16). doi:10.1172/jci.insight.93621
16. Ko F, Muthy ZA, Gallacher J, Sudlow C, Rees G, Yang Q, Keane PA, Petzold A, Khaw PT, Reisman C, Strouthidis NG, Foster PJ, Patel PJ, Eye UKB, Vision C (2018) Association of Retinal Nerve Fiber Layer Thinning With Current and Future Cognitive Decline: A Study Using Optical Coherence Tomography. JAMA Neurol 75 (10):1198-1205. doi:10.1001/jamaneurol.2018.1578
17. Paquet C, Boissonnot M, Roger F, Dighiero P, Gil R, Hugon J (2007) Abnormal retinal thickness in patients with mild cognitive impairment and Alzheimer's disease. Neurosci Lett 420 (2):97-99. doi:10.1016/j.neulet.2007.02.090
18. Sadun AA, Bassi CJ (1990) Optic nerve damage in Alzheimer's disease. Ophthalmology 97 (1):9-17. doi:10.1016/s0161-6420(90)32621-0
19. Lu Y, Li Z, Zhang X, Ming B, Jia J, Wang R, Ma D (2010) Retinal nerve fiber layer structure abnormalities in early Alzheimer's disease: evidence in optical coherence tomography. Neurosci Lett 480 (1):69-72. doi:10.1016/j.neulet.2010.06.006
20. Martersteck EM, Hirokawa KE, Evarts M, Bernard A, Duan X, Li Y, Ng L, Oh SW, Ouellette B, Royall JJ, Stoecklin M, Wang Q, Zeng H, Sanes JR, Harris JA (2017) Diverse Central Projection Patterns of Retinal Ganglion Cells. Cell Rep 18 (8):2058-2072. doi:10.1016/j.celrep.2017.01.075
21. Wienbar S, Schwartz GW (2018) The dynamic receptive fields of retinal ganglion cells. Prog Retin Eye Res 67:102-117. doi:10.1016/j.preteyeres.2018.06.003
22. Monavarfeshani A, Sabbagh U, Fox MA (2017) Not a one-trick pony: Diverse connectivity and functions of the rodent lateral geniculate complex. Vis Neurosci 34:E012. doi:10.1017/S0952523817000098

23. Ahmadlou M, Zweifel LS, Heimel JA (2018) Functional modulation of primary visual cortex by the superior colliculus in the mouse. Nat Commun 9 (1):3895. doi:10.1038/s41467-018-06389-6
24. Ito S, Feldheim DA (2018) The Mouse Superior Colliculus: An Emerging Model for Studying Circuit Formation and Function. Front Neural Circuits 12:10. doi:10.3389/fncir.2018.00010
25. Wurtz RH, Albano JE (1980) Visual-motor function of the primate superior colliculus. Annu Rev Neurosci 3:189-226. doi:10.1146/annurev.ne.03.030180.001201
26. Chen SK, Badea TC, Hattar S (2011) Photoentrainment and pupillary light reflex are mediated by distinct populations of ipRGCs. Nature 476 (7358):92-95. doi:10.1038/nature10206
27. Giannoni P, Gaven F, de Bundel D, Baranger K, Marchetti-Gauthier E, Roman FS, Valjent E, Marin P, Bockaert J, Rivera S, Claeysen S (2013) Early administration of RS 67333, a specific 5-HT4 receptor agonist, prevents amyloidogenesis and behavioral deficits in the 5XFAD mouse model of Alzheimer's disease. Front Aging Neurosci 5:96. doi:10.3389/fnagi.2013.00096
28. Shvarts-Serebro I, Sheinin A, Gottfried I, Adler L, Schottlender N, Ashery U, Barak B (2021) miR-128 as a Regulator of Synaptic Properties in 5xFAD Mice Hippocampal Neurons. J Mol Neurosci 71 (12):2593-2607. doi:10.1007/s12031-021-01862-2
29. Nam Y, Shin SJ, Park YH, Kim MJ, Jeon SG, Lee H, Choi Y, Kim TJ, Shin SM, Kim JJ, Yoo DH, Kim HD, Kim S, Moon M (2021) Platycodon grandiflorum Root Protects against Abeta-Induced Cognitive Dysfunction and Pathology in Female Models of Alzheimer's Disease. Antioxidants (Basel) 10 (2). doi:10.3390/antiox10020207
30. Grant RA, Wong AA, Fertan E, Brown RE (2020) Whisker exploration behaviours in the 5xFAD mouse are affected by sex and retinal degeneration. Genes Brain Behav 19 (3):e12532. doi:10.1111/gbb.12532
31. Chang B, Hawes NL, Hurd RE, Davisson MT, Nusinowitz S, Heckenlively JR (2002) Retinal degeneration mutants in the mouse. Vision Res 42 (4):517-525. doi:10.1016/s0042-6989(01)00146-8
32. Park SW, Kim JH, Park SM, Moon M, Lee KH, Park KH, Park WJ, Kim JH (2015) RAGE mediated intracellular Abeta uptake contributes to the breakdown of tight junction in retinal pigment epithelium. Oncotarget 6 (34):35263-35273. doi:10.18632/oncotarget.5894
33. Welsh DK, Takahashi JS, Kay SA (2010) Suprachiasmatic nucleus: cell autonomy and network properties. Annu Rev Physiol 72:551-577. doi:10.1146/annurev-physiol-021909-135919
34. Fernandez DC, Chang YT, Hattar S, Chen SK (2016) Architecture of retinal projections to the central circadian pacemaker. Proc Natl Acad Sci U S A 113 (21):6047-6052. doi:10.1073/pnas.1523629113
35. Sonoda T, Li JY, Hayes NW, Chan JC, Okabe Y, Belin S, Nawabi H, Schmidt TM (2020) A noncanonical inhibitory circuit dampens behavioral sensitivity to light. Science 368 (6490):527-531. doi:10.1126/science.aay3152
36. Derrington A (2001) The lateral geniculate nucleus. Current Biology 11 (16):R635-R637. doi:10.1016/S0960-9822(01)00379-7
37. Tohmi M, Meguro R, Tsukano H, Hishida R, Shibuki K (2014) The extrageniculate visual pathway generates distinct response properties in the higher visual areas of mice. Curr Biol 24 (6):587-597.

doi:10.1016/j.cub.2014.01.061

38. Nishioka C, Poh C, Sun SW (2015) Diffusion tensor imaging reveals visual pathway damage in patients with mild cognitive impairment and Alzheimer's disease. J Alzheimers Dis 45 (1):97-107. doi:10.3233/JAD-141239
39. Palop JJ, Mucke L (2010) Amyloid-beta-induced neuronal dysfunction in Alzheimer's disease: from synapses toward neural networks. Nat Neurosci 13 (7):812-818. doi:10.1038/nn.2583
40. Alobuia WM, Xia W, Vohra BP (2013) Axon degeneration is key component of neuronal death in amyloid-beta toxicity. Neurochem Int 63 (8):782-789. doi:10.1016/j.neuint.2013.08.013
41. Van Erum J, Van Dam D, De Deyn PP (2018) Sleep and Alzheimer's disease: A pivotal role for the suprachiasmatic nucleus. Sleep Med Rev 40:17-27. doi:10.1016/j.smrv.2017.07.005
42. Sethi M, Joshi SS, Webb RL, Beckett TL, Donohue KD, Murphy MP, O'Hara BF, Duncan MJ (2015) Increased fragmentation of sleep-wake cycles in the 5XFAD mouse model of Alzheimer's disease. Neuroscience 290:80-89. doi:10.1016/j.neuroscience.2015.01.035
43. Hastings MH, Maywood ES, Brancaccio M (2018) Generation of circadian rhythms in the suprachiasmatic nucleus. Nat Rev Neurosci 19 (8):453-469. doi:10.1038/s41583-018-0026-z
44. Lewandowski MH, Usarek A (2002) Effects of intergeniculate leaflet lesions on circadian rhythms in the mouse. Behav Brain Res 128 (1):13-17. doi:10.1016/s0166-4328(01)00264-9
45. Lennie P, Perry VH (1981) Spatial contrast sensitivity of cells in the lateral geniculate nucleus of the rat. J Physiol 315:69-79. doi:10.1113/jphysiol.1981.sp013733
46. Schiller PH, Malpeli JG (1978) Functional specificity of lateral geniculate nucleus laminae of the rhesus monkey. J Neurophysiol 41 (3):788-797. doi:10.1152/jn.1978.41.3.788
47. Salobrar-Garcia E, de Hoz R, Ramirez AI, Lopez-Cuenca I, Rojas P, Vazirani R, Amarante C, Yubero R, Gil P, Pinazo-Duran MD, Salazar JJ, Ramirez JM (2019) Changes in visual function and retinal structure in the progression of Alzheimer's disease. PLoS One 14 (8):e0220535. doi:10.1371/journal.pone.0220535
48. Salobrar-Garcia E, de Hoz R, Rojas B, Ramirez AI, Salazar JJ, Yubero R, Gil P, Trivino A, Ramirez JM (2015) Ophthalmologic Psychophysical Tests Support OCT Findings in Mild Alzheimer's Disease. J Ophthalmol 2015:736949. doi:10.1155/2015/736949
49. Vit JP, Fuchs DT, Angel A, Levy A, Lamensdorf I, Black KL, Koronyo Y, Koronyo-Hamaoui M (2021) Color and contrast vision in mouse models of aging and Alzheimer's disease using a novel visual-stimuli four-arm maze. Sci Rep 11 (1):1255. doi:10.1038/s41598-021-80988-0
50. Zhang M, Zhong L, Han X, Xiong G, Xu D, Zhang S, Cheng H, Chiu K, Xu Y (2021) Brain and Retinal Abnormalities in the 5xFAD Mouse Model of Alzheimer's Disease at Early Stages. Front Neurosci 15:681831. doi:10.3389/fnins.2021.681831
51. Osterhout JA, Josten N, Yamada J, Pan F, Wu SW, Nguyen PL, Panagiotakos G, Inoue YU, Egusa SF, Volgyi B, Inoue T, Bloomfield SA, Barres BA, Berson DM, Feldheim DA, Huberman AD (2011) Cadherin-6 mediates axon-target matching in a non-image-forming visual circuit. Neuron 71 (4):632-639. doi:10.1016/j.neuron.2011.07.006

52. Sperling RA, Aisen PS, Beckett LA, Bennett DA, Craft S, Fagan AM, Iwatsubo T, Jack CR, Jr., Kaye J, Montine TJ, Park DC, Reiman EM, Rowe CC, Siemers E, Stern Y, Yaffe K, Carrillo MC, Thies B, Morrison-Bogorad M, Wagster MV, Phelps CH (2011) Toward defining the preclinical stages of Alzheimer's disease: recommendations from the National Institute on Aging-Alzheimer's Association workgroups on diagnostic guidelines for Alzheimer's disease. Alzheimers Dement 7 (3):280-292. doi:10.1016/j.jalz.2011.03.003
53. Bargagli A, Fontanelli E, Zanca D, Castelli I, Rosini F, Maddii S, Di Donato I, Carluccio A, Battisti C, Tosi GM, Dotti MT, Rufa A (2020) Neurophthalmologic and Orthoptic Ambulatory Assessments Reveal Ocular and Visual Changes in Patients With Early Alzheimer and Parkinson's Disease. Front Neurol 11:577362. doi:10.3389/fneur.2020.577362
54. Ngolab J, Honma P, Rissman RA (2019) Reflections on the Utility of the Retina as a Biomarker for Alzheimer's Disease: A Literature Review. Neurol Ther 8 (Suppl 2):57-72. doi:10.1007/s40120-019-00173-4
55. Bokde AL, Lopez-Bayo P, Born C, Ewers M, Meindl T, Teipel SJ, Faltraco F, Reiser MF, Moller HJ, Hampel H (2010) Alzheimer disease: functional abnormalities in the dorsal visual pathway. Radiology 254 (1):219-226. doi:10.1148/radiol.2541090558
56. Krasodomska K, Lubinski W, Potemkowski A, Honczarenko K (2010) Pattern electroretinogram (PERG) and pattern visual evoked potential (PVEP) in the early stages of Alzheimer's disease. Doc Ophthalmol 121 (2):111-121. doi:10.1007/s10633-010-9238-x
57. Risacher SL, Wudunn D, Pepin SM, MaGee TR, McDonald BC, Flashman LA, Wishart HA, Pixley HS, Rabin LA, Pare N, Englert JJ, Schwartz E, Curtain JR, West JD, O'Neill DP, Santulli RB, Newman RW, Saykin AJ (2013) Visual contrast sensitivity in Alzheimer's disease, mild cognitive impairment, and older adults with cognitive complaints. Neurobiol Aging 34 (4):1133-1144. doi:10.1016/j.neurobiolaging.2012.08.007
58. Rizzo M, Anderson SW, Dawson J, Nawrot M (2000) Vision and cognition in Alzheimer's disease. Neuropsychologia 38 (8):1157-1169. doi:10.1016/s0028-3932(00)00023-3
59. Thoreson WB, Witkovsky P (1999) Glutamate receptors and circuits in the vertebrate retina. Prog Retin Eye Res 18 (6):765-810. doi:10.1016/s1350-9462(98)00031-7
60. Xu X, Holmes TC, Luo MH, Beier KT, Horwitz GD, Zhao F, Zeng W, Hui M, Semler BL, Sandri-Goldin RM (2020) Viral Vectors for Neural Circuit Mapping and Recent Advances in Trans-synaptic Anterograde Tracers. Neuron 107 (6):1029-1047. doi:10.1016/j.neuron.2020.07.010
61. Alexandrov PN, Pogue A, Bhattacharjee S, Lukiw WJ (2011) Retinal amyloid peptides and complement factor H in transgenic models of Alzheimer's disease. Neuroreport 22 (12):623-627. doi:10.1097/WNR.0b013e3283497334
62. Parthasarathy R, Chow KM, Derafshi Z, Fautsch MP, Hetling JR, Rodgers DW, Hersh LB, Pepperberg DR (2015) Reduction of amyloid-beta levels in mouse eye tissues by intra-vitreally delivered neprilysin. Exp Eye Res 138:134-144. doi:10.1016/j.exer.2015.06.027

63. Pogue AI, Dua P, Hill JM, Lukiw WJ (2015) Progressive inflammatory pathology in the retina of aluminum-fed 5xFAD transgenic mice. J Inorg Biochem 152:206-209. doi:10.1016/j.jinorgbio.2015.07.009

Figures

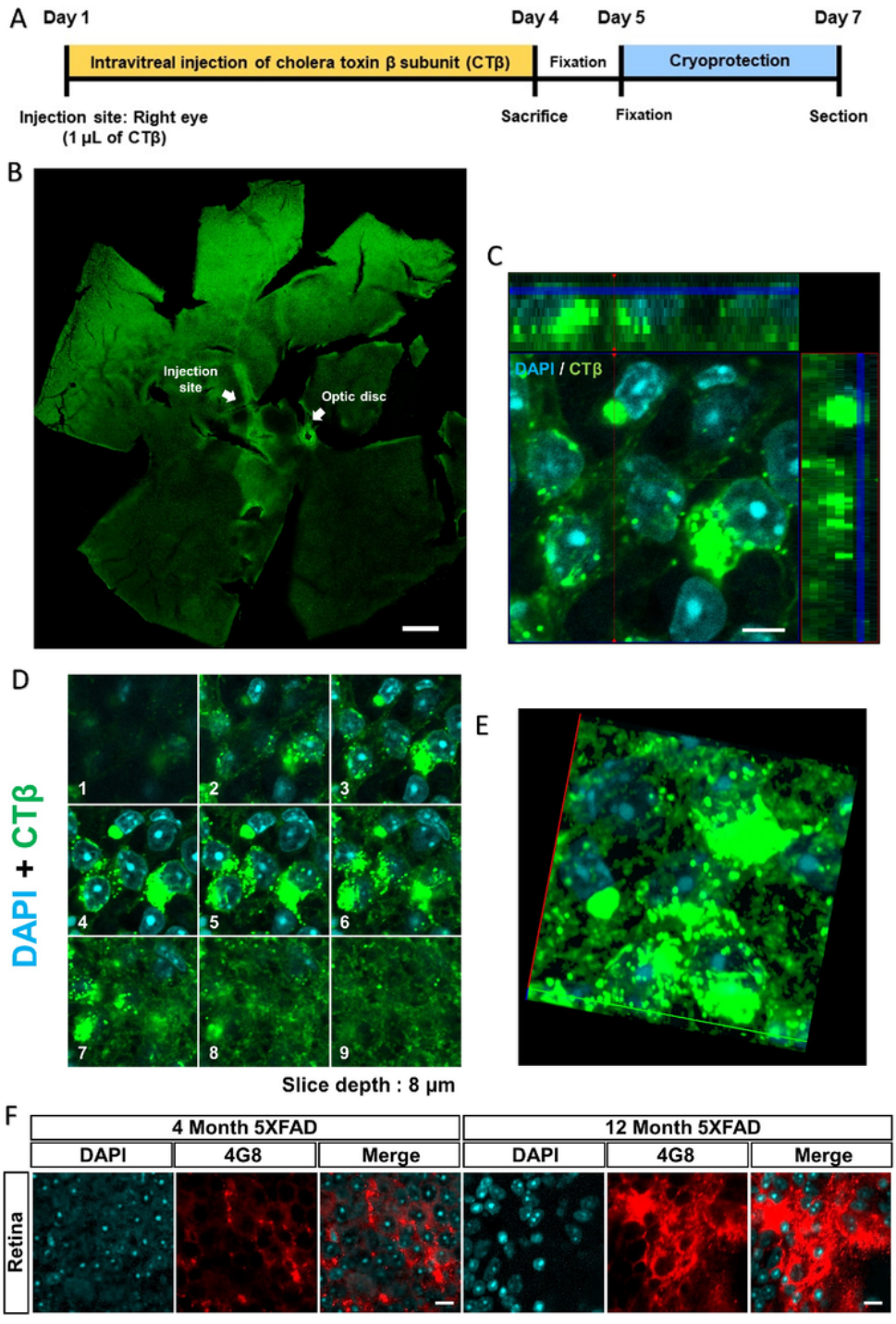

Figure 1

Validation of the application of cholera toxin β subunit (CTβ) and characterization of amyloid-β (Aβ) deposition in the retina of wild type (WT) and 5XFAD mice. (A) The schematic diagram shows the overall experimental design. (B) Representative image of the photomicrograph validation of the intravitreal injection sites of the CTβ in the retinal flat mount of the WT and 5XFAD mice. Scale bar = 500 μm. (C) An orthogonal view of the z-stack images indicates that the CTβ has an intracellular localization in retinal cells. The side and bottom panels, respectively, depict y–z and x–z cross-sectional images. Scale bar = 5 μm. (D) Serial z-stack images consist of 9 sections at 1-μm intervals. (E) The representative image shows a three-dimensional z-projection of the acquired stack. (F) The representative image shows Aβ accumulation in the retina by immunohistochsemical staining with anti-4G8 antibody. Scale bar = 10 μm.

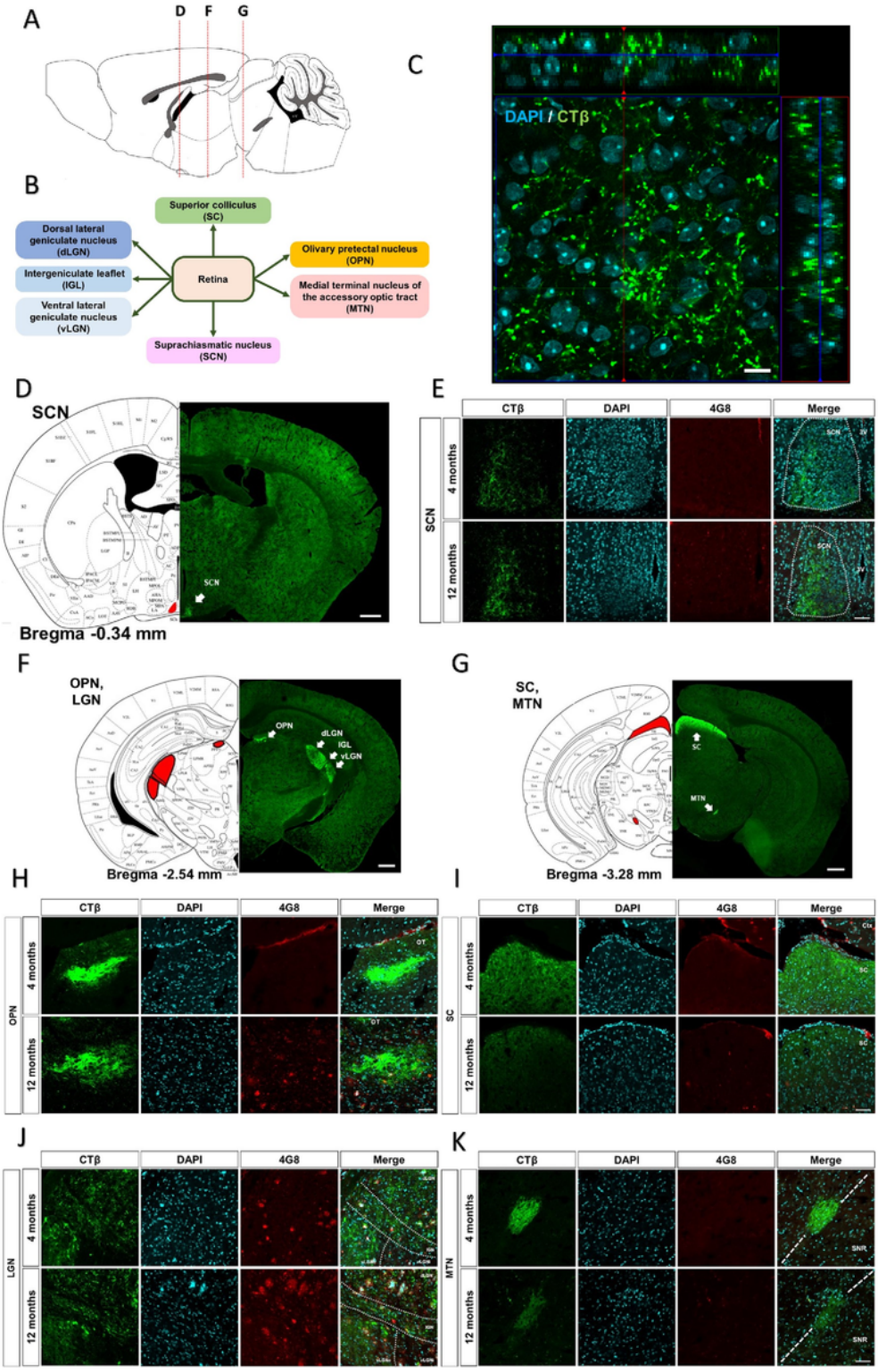

Figure 2

Histological profiling of the CTβ and amyloid-β (Aβ) deposition in the retinorecipient regions of WT and 5XFAD mice. (A) The sagittal plane of the mouse brain indicates the positions of the representative Fig.s in D, F, and G. (B) The schematic diagram indicates the projection from the retina to the retinorecipient regions of the brain. CTβ-positive signals represent the retinal output to the (D) SCN, (F) OPN/LGN, and (G) SC/MTN in the brain hemisphere. Scale bar = 500 μm. (C) The representative orthogonal view shows

that the CTβ is localized to the terminal buttons of the axon in the SCN of 4-monthe WT mice. The side and bottom panels, respectively, depict the y–z and x–z cross-sectional images. Scale bar = 10 μm. Representative images show the deposition of Aβ plaques stained with 4G8 antibody in the (E) SCN, (H) OPN, (I) SC, (J) LGN, and (K) MTN of 4- and 12-month-old 5XFAD groups. Scale bar = 50 μm. LGN, lateral geniculate nucleus; MTN, medial terminal nucleus of the accessory optic tract; OPN, olivary pretectal nucleus; SC, superior colliculus; SCN, suprachiasmatic nucleus.

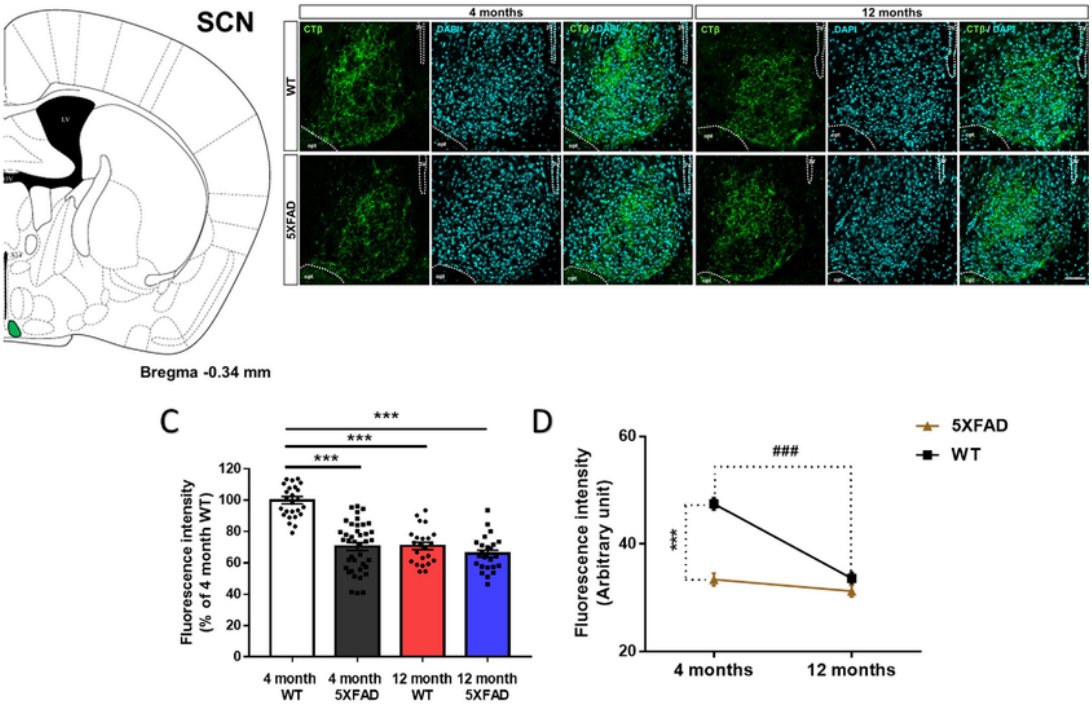

Figure 3

Impairment of the retina-suprachiasmatic nucleus (SCN) pathway in WT and 5XFAD mice. (A) Diagram of a mouse brain section explaining the location of the SCN. (B) The representative image shows CTβ-labeled terminal buttons of the axon in the SCN of 4- and 12-month-old WT and 5XFAD mice. Scale bar = 50 μm. (C) The quantitative graph exhibits the fluorescence intensity of the CTβ (+) area in the SCN of WT and 5XFAD mice. (D) Comparison of the impairment of the retina-SCN pathway by aging and AD progression. *** $p < 0.001$ and $^{###}p < 0.001$ indicate a significant difference.

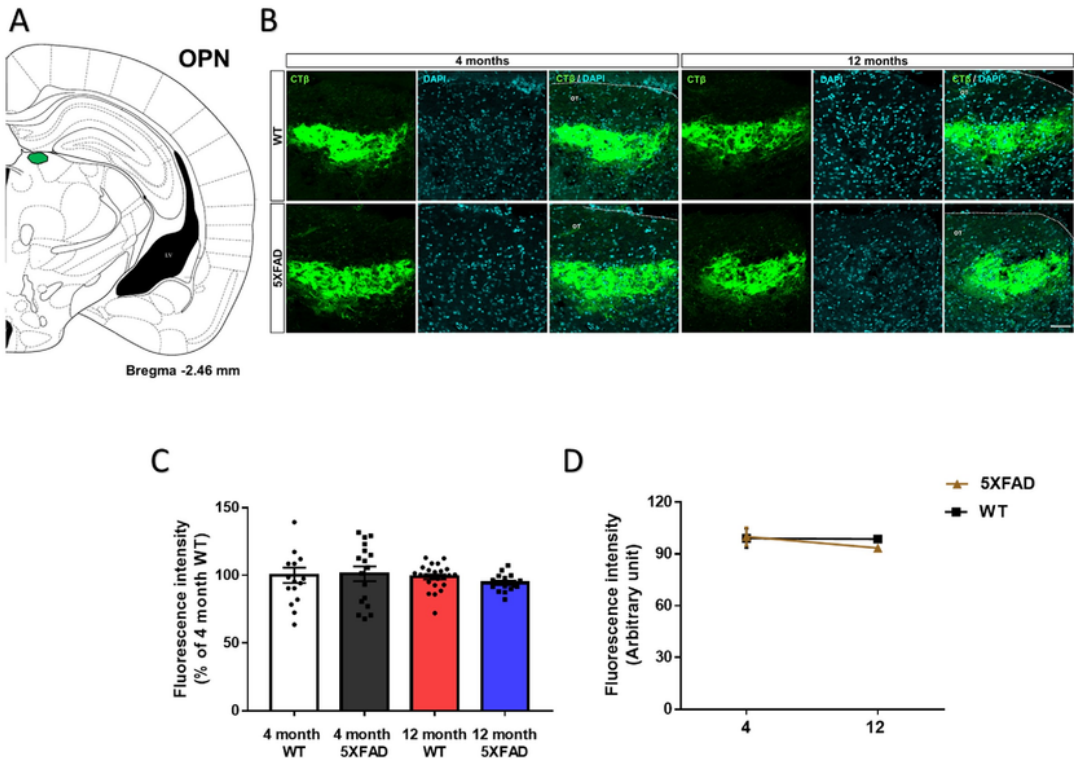

Figure 4

Anatomical tracing of the retina-olivary pretectal nucleus (OPN) pathways in WT and 5XFAD mice. (A) Diagram of a mouse brain section illustrating the location of the OPN. (B) The representative images show CTβ transported from the retina to the OPN. The scale bars are 50 and 500 μm, respectively. (C) The quantitative graphs exhibit the fluorescence intensity of the CTβ (+) areas in the OPN of the WT and

5XFAD mice. (D) Comparison of the impairment of the retina-OPN projection by aging and AD progression.

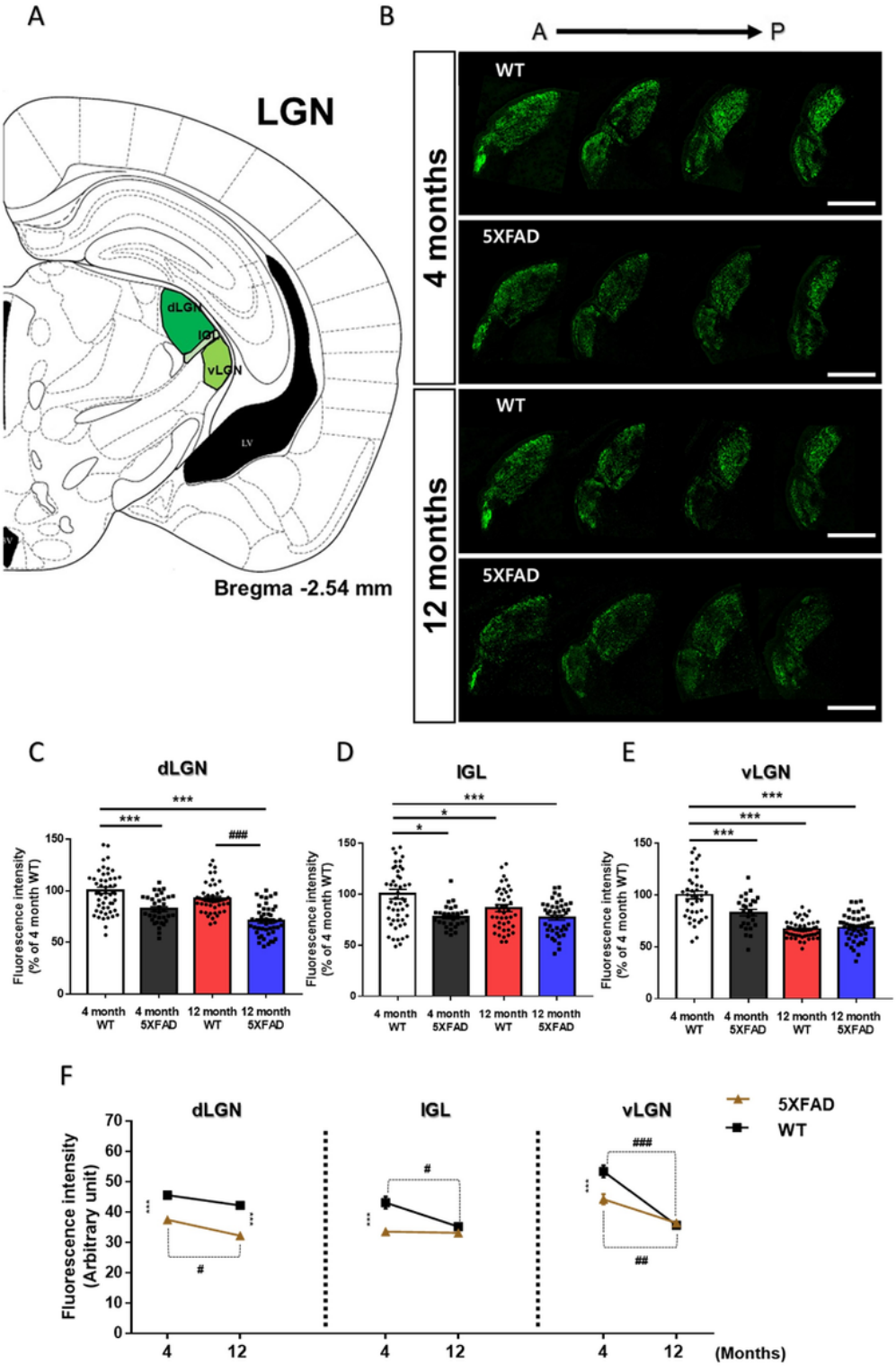

Figure 5

Changes of the retina-lateral geniculate nucleus (LGN) connections in WT and 5XFAD mice. (A) Image of a mouse brain atlas exhibiting the location of the LGN. (B) The representative images show CTβ

transported from the retina to the LGN. The scale bars are 50 and 500 μm, respectively. The quantitative graphs exhibit the fluorescence intensity of CTβ (+) areas in the (C) dorsal lateral geniculate nucleus (dLGN), (D) intergeniculate leaflet (IGL), and the (E) ventral lateral geniculate nucleus (vLGN) of WT and 5XFAD mice. (F) Comparison of the impairment of the retina- LGN pathways by aging and AD progression. * $p < 0.05$, *** $p < 0.001$, # $p < 0.05$, ## $p < 0.01$, and ### $p < 0.001$ indicate a significant difference.

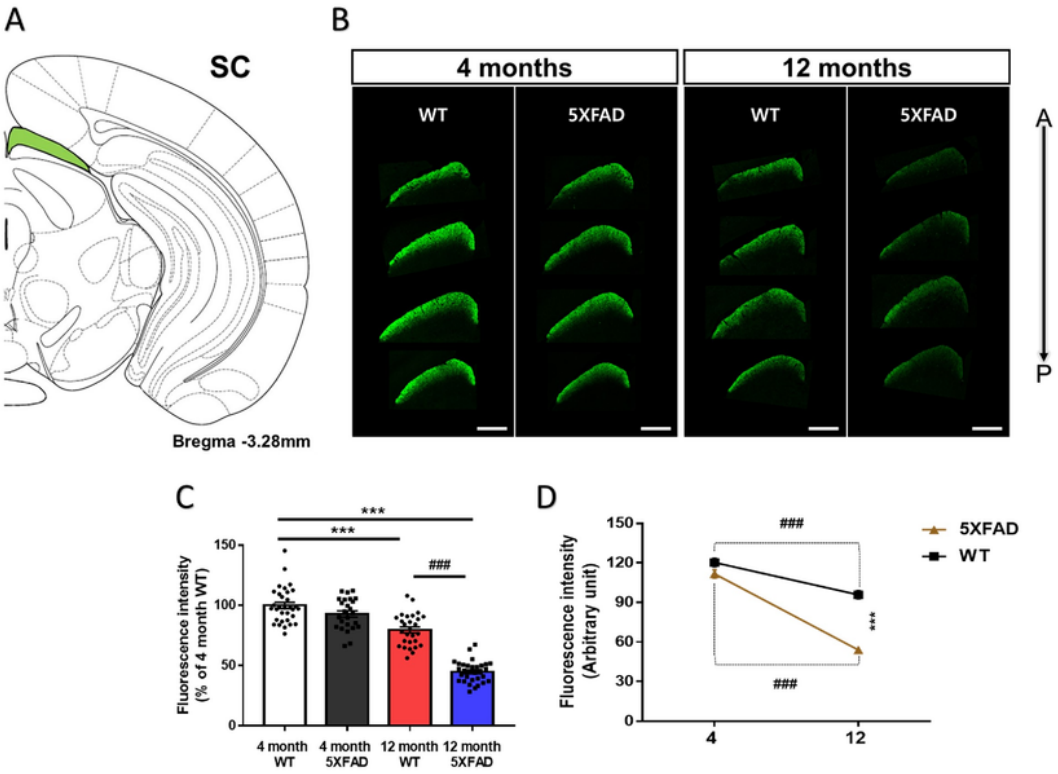

Figure 6

Degeneration of the retina-superior colliculus (SC) pathways in WT and 5XFAD mice. (A) Image of a mouse brain atlas illustrating the location of the SC. (B) The representative images indicate CTβ transported from the retina to the SC. The scale bars are 500 and 50 μm, respectively. (C) The quantitative graphs exhibit the fluorescence intensity of CTβ (+) areas in the SC of WT and 5XFAD mice. (D) Comparison of the impairment of the retina-SC connection by aging and AD progression. $^{***}p < 0.001$ and $^{###}p < 0.001$ indicate a significant difference.

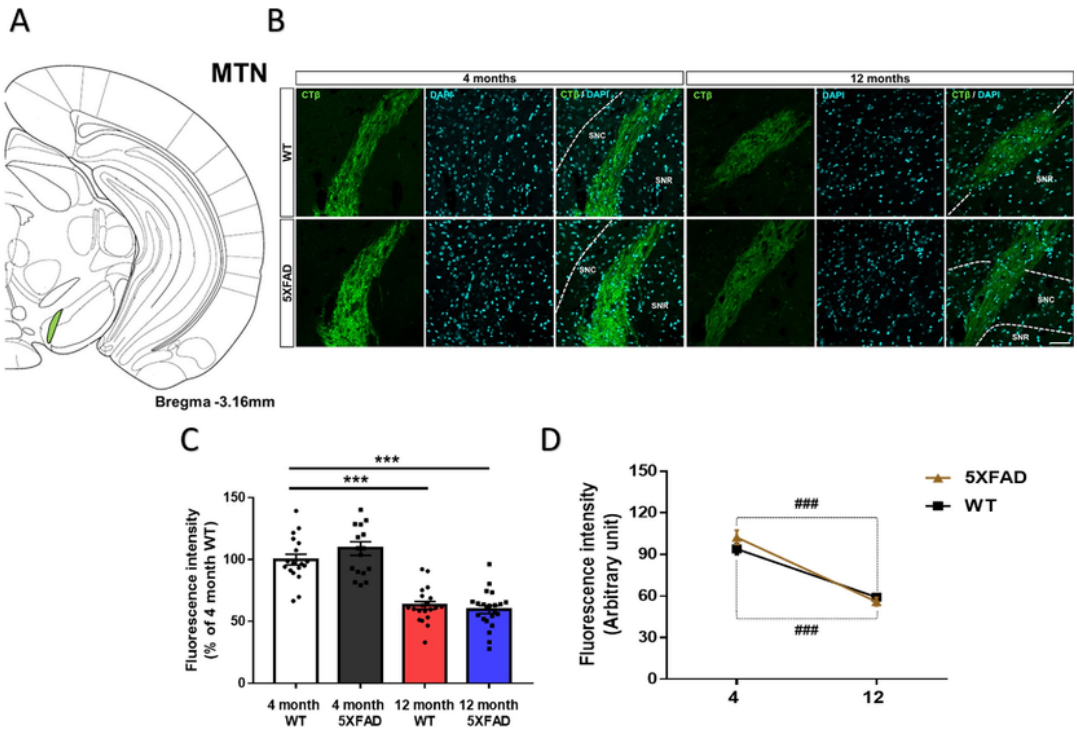

Figure 7

Neuroanatomic tract tracing of the retina-medial terminal nucleus of the accessory optic tract (MTN) projections in WT and 5XFAD mice. (A) Diagram of a mouse brain atlas illustrating the site of the MTN. (B) The representative images indicate CTβ transported from the retina to the MTN. The scale bars are 500 and 50 μm, respectively. (C) The quantitative graphs exhibit the fluorescence intensity of CTβ (+)

areas in the MTN of WT and 5XFAD mice. (D) Comparison of the impairment of the retina-MTN pathways by aging and AD progression. *** $p < 0.001$ and ### $p < 0.001$ indicate a significant difference.

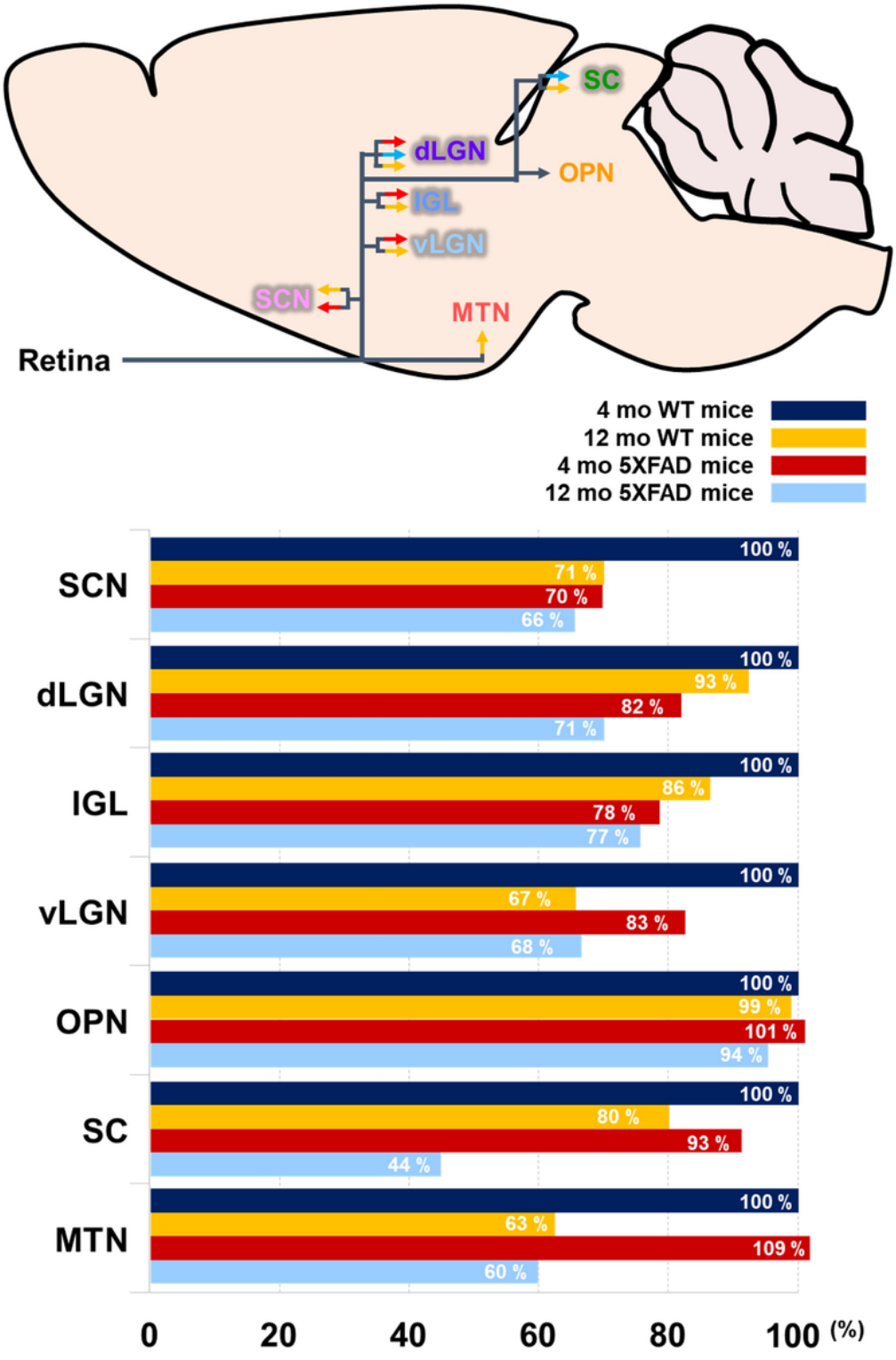

Figure 8

Schematic drawing and quantitative analysis of the altered visual pathways from the retina to the retinorecipient regions. The rate of degeneration of the visual pathways was normalized to those of 4-

month-old WT mice indicated by the black bars. Red bars displayed regions that are impaired in early-stage of AD. Blue bars indicate the damaged regions in late-stage of AD. Orange bars show regions damaged by aging.